

Flow Patterns of Cellular Automata and Optimal-velocity Traffic Models at Highway Bottlenecks

Peter BERG¹ and Justin FINDLAY

Faculty of Science, University of Ontario Institute of Technology,
2000 Simcoe Street N., Oshawa, ON, L1H 7K4, Canada,

¹Email: peter.berg@uoit.ca, Phone: +1 905 721 8668,
FAX: +1 905 721 3304, web: www.peterberg.net

16 July 2007

Abstract

A bottleneck simulation of road traffic on a loop, using the deterministic cellular automata (CA) Nagel-Schreckenberg model with zero dawdling probability, reveals three types of stationary wave solutions. They consist of i) two shock waves, one at each bottleneck boundary, ii) one shock wave at the boundary and one on the “open” road, and iii) the trivial solution, i.e. homogeneous, uniform flow. These solutions are selected dynamically from a range of kinematically permissible stationary shocks. This is similar in fashion to the wave selection in a bottleneck simulation of the optimal-velocity (OV) model, which is explained by a travelling wave phase-plane analysis of the corresponding continuum model. It is yet another strong indication that CA and OV models share certain underlying dynamics, although the former are discrete in space and time while the latter are continuous.

Keywords: Traffic flow, bottleneck, cellular automata, Nagel-Schreckenberg model, optimal velocity, pattern formation

1 Introduction

Cellular automata (CA) models have been widely used to simulate traffic flow on highways and road networks [1, 2, 3, 4, 5, 6, 7, 8, 9], in particular the Nagel-Schreckenberg model [10, 11]. Together with car-following (CF) and continuum models, they represent the three predominant classes of traffic models.

Analytical work by Berg *et al.* [12] and Lee *et al.* [13] has established a link between car-following models based on ordinary differential equations, and continuum models based on partial differential equations. While an analytical link between CA models and either CF or continuum models is still missing (mean-field theory aside), the dynamics of all three classes exhibit many common features such as sub-critical bifurcations, limit cycles and pattern formation [14, 15].

Bottlenecks are the major cause for highway congestion and, therefore, have been studied in some detail [16, 17, 18, 19, 20, 21]. In this paper, a wave selection analysis of a bottleneck simulation reveals a fundamental link between the dynamics of CA models and optimal-velocity (OV) models [22], which belong to the class of CF models.

The paper is organised as follows. We begin with the description of the CA bottleneck simulation in section 2. Section 3 presents the resulting wave patterns and how they can be interpreted in the fundamental diagram. In the thermodynamic limit, boundaries between the different wave regimes are computed. Section 4 briefly addresses the impact of the dawdling probability on the effective fundamental diagram.

Section 5 discusses a bottleneck simulation in the car-following OV model, resulting in identical wave patterns as compared to the CA model. In contrast to the CA model, analytical tools can be applied to explain the wave selections. In particular, continuum theory is used to investigate travelling waves in terms of plateau connections between equilibrium flow solutions. A strong link between CA and OV models emerges.

Finally, some of the results are compared to work in the literature which is related to bottleneck simulations (section 6), before we draw some conclusions and mention planned future work in the last section.

2 Cellular Automata bottleneck simulation

For traffic on a loop (periodic boundary conditions) of length L , a bottleneck of length L_B is located at $0 \leq x \leq L_B$ (Fig. 1). The system is simulated

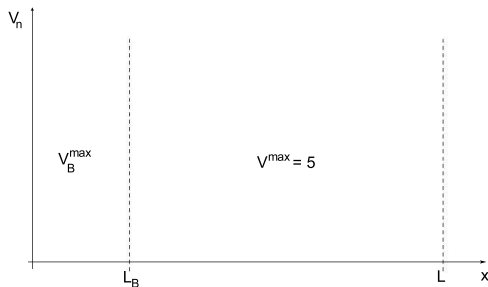


Figure 1: The bottleneck simulation assumes periodic boundary conditions (traffic on a loop). The “open” road ($L_B < x \leq L$) is modeled with the conventional Nagel-Schreckenberg model [10]. The bottleneck ($0 \leq x \leq L_B$) uses the same model except for a smaller maximum speed v_B^{max} . In the simulations, we set $L_B = 200$ and $L = 1000$.

with the Nagel-Schreckenberg (NS) CA model [10] for vanishing randomness ($p = 0$) and a reduction in top speed from $v^{max} = 5$ on the “open” road to $v_B^{max} = 3$ in the bottleneck. All other model parameters remain the same. Initially, N cars are randomly distributed along the road and the system is updated up to $t = 10^6$ time steps. We set $L_B = 200$ and $L = 1000$ and study the emerging wave patterns. We also choose $p = 0$ in order to avoid the jam formation in the NS model, which would interfere with the stationary wave patterns and complicate the analysis.

Figure 2 is a qualitative plot of the equilibrium velocity function used in the update rule of the NS CA model for both the bottleneck and the open road. Here, $h' = 1$, $v^{max} = 5$ and $v_B^{max} = 3$. Since the density ρ is continuous in this plot but the CA model is discrete in space, ρ must be interpreted in the thermodynamic limit as an average density taken over many cells.

Note that the wave selection on a loop is fundamentally different from wave selection on an open road with different conditions at the upstream and downstream boundary, respectively [5, 6, 8]. On an open road, travelling waves can only interact once with stationary structures since they do not move around a loop. Therefore, an open road gives rise to new wave solutions as compared to the loop, determined by the boundary conditions [5, 6, 8]. This is a very different setup from what is presented in this work.

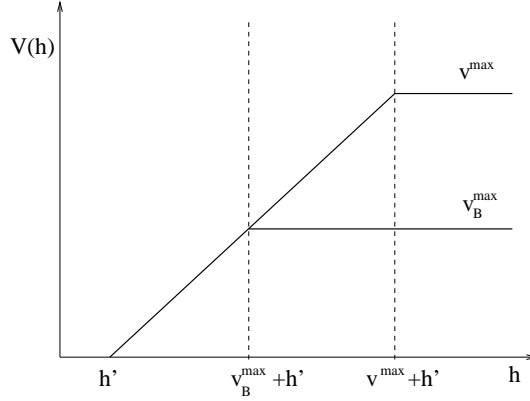


Figure 2: The equilibrium velocity function of the CA model, velocity V as a function of the headway h (distance) between the cars. It is a piecewise linear function in the bottleneck and on the open road with an upper bound of v^{max} on the open road and v_B^{max} in the bottleneck. The functions are partially identical which translates into partially identical fundamental diagrams (see Fig. 3). Here, h' represents the minimum distance between the cars.

3 Wave selection in the fundamental diagram

We will use the fundamental diagram (FD), i.e. flux versus density, and kinematic wave theory to interpret our numerical results. Based on the equilibrium velocity function in Fig. 2 and using the equilibrium flow-density relation of uniform flow (q : flux, ρ : density)

$$q = v(\rho) \rho, \quad \rho = 1/h, \quad (1)$$

the FD is shown for both the bottleneck

$$q_B = \begin{cases} 3\rho & ; \quad 0 \leq \rho \leq 1/4, \\ 1 - \rho & ; \quad 1/4 < \rho \leq 1 \end{cases} \quad (2)$$

and the open road

$$q_o = \begin{cases} 5\rho & ; \quad 0 \leq \rho \leq 1/6, \\ 1 - \rho & ; \quad 1/6 < \rho \leq 1 \end{cases} \quad (3)$$

in Fig. 3. The two curves merge into the same function for $\rho \geq 1/4$.

Generally speaking, we could expect as many as six stationary wave solutions for a bottleneck on a loop as $t \rightarrow \infty$. In the FD, five of them are

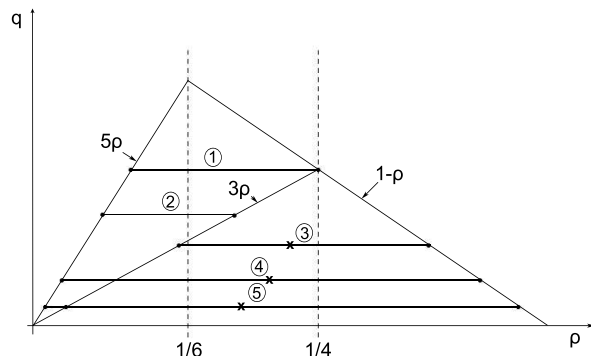


Figure 3: Stationary shock waves visualized in the fundamental diagram: From six possible wave connections (the trivial uniform flow solution in Figs. 7 and 8 is not shown here), only three emerge as dynamical solutions, displayed in Figs. 5-8.

visualized as chords with zero gradient due to the requirement of vanishing wave speed, based on kinematic wave theory [20]. By kinematic waves we refer to density waves described by the first-order hyperbolic Lighthill-Whitham model of traffic flow [23]

$$\rho_t + q(\rho)_x = 0 \Rightarrow \rho_t + q'(\rho)\rho_x = 0. \quad (4)$$

For stationary waves, we have $\rho_t = 0$ and the equation can be integrated to yield

$$q(\rho(x)) = \text{const}. \quad (5)$$

Therefore, stationary shock waves, whose profiles are given by $\rho(x)$, exhibit constant flux along the road, represented by a horizontal straight line in the fundamental diagram. In Fig. 3, each chord is a straight line between points on the fundamental diagrams, one point representing the bottleneck and one representing the open-road FD. They connect plateaus between the bottleneck and the open road (case 2, 3 and 4) in case of one stationary shock wave at each bottleneck boundary. However, they can also entail a plateau connection on the open road as in cases 1 and 5. These five stationary wave patterns are shown in Fig. 4 in terms of density distribution along the loop. In addition, there is the trivial wave solution of homogeneous uniform flow. In principle, we could think of further wave patterns but we will restrict the analysis to the simplest cases featured here.

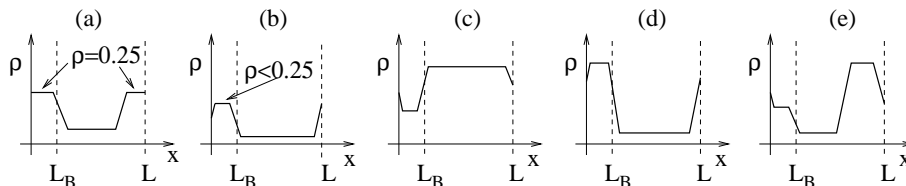


Figure 4: Stationary wave patterns of Fig. 3. While cases (a) and (b) occur in the simulations (cases (1) and (2) in Fig. 3), as shown in Figs. 5 and 6, cases (c), (d), and (e) do not emerge. This is a very close analogy to the wave pattern selection of a bottleneck simulation with the optimal-velocity model (see section 5) [24, 25].

We found in our simulations that only three wave patterns are selected from this range of possible solutions. They consist of the following (ρ : average density on the loop):

- Case 1: $0.17 \leq \rho < 0.25$

Stationary wave pattern that connects two plateaus by one shock at the downstream boundary of the bottleneck and one classical (Lax) shock on the open road (see Figs. 4a and 5): The resulting bottleneck headway (distance between cars) is exactly at $d_B = 4$ and, therefore, the bottleneck is at maximum flow. On the open road we find the headway to be near $d_n = 7$, or exactly $d_o = 20/3$ on average.

- Case 2: $0 \leq \rho < 0.17$

Stationary wave pattern that connects two plateaus by a shock at the upstream and downstream boundary of the bottleneck, respectively (see Fig. 4b and 6): In the bottleneck $d_B > 4$ and on the open road $d_o > 20/3$. It shall be stressed that it takes a very long time for the system to reach steady-state due to the small interaction of cars on the open road. Hence, Fig. 6 should be considered as a transient, quasi-steady state.

- Case 3: $\rho > 0.25$

Trivial flow solution, i.e. homogeneous, uniform flow: Unless the average headway d is close to an integer number, as is the case in Fig. 7, the individual headways d_n oscillate around the average headway d , exhibited in Fig. 8. However, this is an effect solely due to the discretization of space, and the flow solution can still be considered uniform. In

particular, the average flow measured in Fig. 8, $q = 0.55$, equals exactly the uniform flow in the FD, as expected from an average density $\rho = 0.45$, namely $q = 1 - \rho = 0.55$.

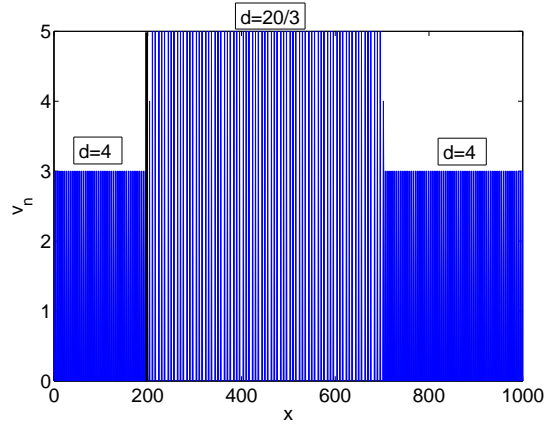


Figure 5: Stationary wave pattern of bottleneck simulation with average density $0.17 < \rho < 0.25$ (here: $\rho = 0.20$): Two shocks emerge, one at the downstream bottleneck boundary and one classical (Lax) shock on the open road. The flow in the bottleneck is at its maximum.

This leads to three open questions:

1. Why is there a transition between the structures at $\rho = 0.17$ and $\rho = 0.25$?
2. What determines the location of the classical shock on the open road in case 1?
3. Why do we not observe the other wave patterns?

We will now elaborate on all three questions.

The two headways in Fig. 6 are determined by the conservation of cars and by imposing zero wave speed (zero gradient of the chord in the FD), described by Eq. (5). This can be written as two equations with two unknowns, the bottleneck headway d_B and the open-road headway d_o . Neglecting finite size effects, conservation of cars reads

$$\frac{L - L_B}{d_o} + \frac{L_B}{d_B} = N. \quad (6)$$

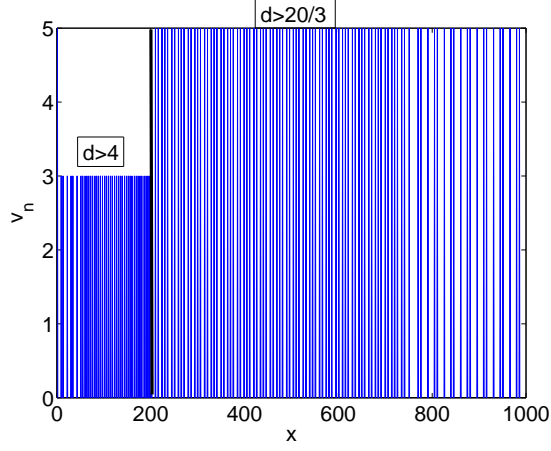


Figure 6: Stationary wave pattern of bottleneck simulation with average density $\rho < 0.17$ (here: $\rho = 0.142$): Two shocks emerge, one at each bottleneck boundary.

We find for the wave speed criterion (equal fluxes q_B and q_o in both road segments)

$$q_B = q_o \Rightarrow 3\rho_B = 5\rho_o \Rightarrow \frac{3}{d_B} = \frac{5}{d_o}, \quad (7)$$

where ρ_B and ρ_o denote the bottleneck and open-road density, respectively.

The system (6)-(7) can be solved for d_B . It yields

$$d_B = \frac{\frac{3}{5}L + \frac{2}{5}L_B}{N}. \quad (8)$$

In Fig. 6, we have $L = 1000$, $L_B = 200$, $N = 142$ and, hence, $d_B = 4.79$. This equals $\rho_B = 1/d_B = 0.21$, which coincides with the numerical value. The value for d_o follows correspondingly.

The maximum amount of vehicles that the wave structure in Fig. 6 can support, however, is reached when $d_B = 4.0$ and, determined by zero wave speed, $d_o = 20/3$. For $L_B = 200$, this corresponds to an average density of

$$\rho = 0.2\frac{1}{4} + 0.8\frac{1}{20/3} = 0.17. \quad (9)$$

This is coincidentally close to $q = 1/6$, the maximum of q_o , but varies with the choice of L_B . If we increase ρ beyond this, the wave pattern in Fig. 5 is

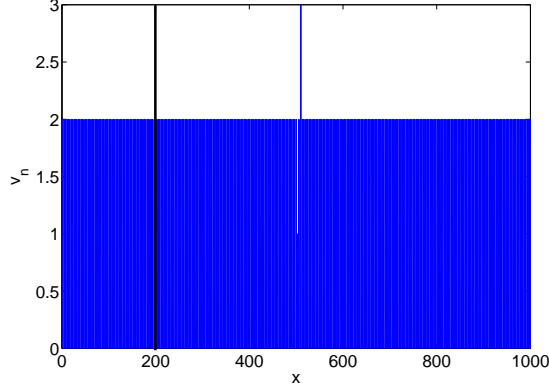


Figure 7: Trivial flow solution for bottleneck simulation with average density $\rho > 0.25$ (here: $\rho = 0.333 \Rightarrow d \approx 3$).

triggered, with a bottleneck headway exactly at $d_B = 4$ and $d_o = 20/3$ for the other plateau value. This is shown by chord 1 in Fig. 3. The length of the second plateau L_p is now determined by the conservation of cars alone. Setting $\rho = 0.2$ in Fig. 5, we write

$$\rho = \frac{1}{4}(1 - L_p/L) + \frac{1}{20/3}(L_p/L) \Rightarrow L_p = 500, \quad (10)$$

which is very close to the numerical value of $L \approx 510$. Note that finite size effects impose limits on the accuracy of estimates. For $\rho \geq 0.25$, which is the maximum of q_B , the length L_p of the open-road plateau equals zero and this wave pattern must vanish. We are left with the trivial flow solution of Figs. 7 and 8 since the average density exceeds the maximum density that can support the wave structure in Fig. 5.

Thus, we have answered questions 1 and 2. Before we turn to question 3 in section 5, let us study the effective fundamental diagrams obtained in the simulations. Here, we will only briefly discuss the impact of $p > 0$ on the fundamental diagram and leave a more detailed study to future research.

4 Impact of the dawdling probability on the fundamental diagram

The well-defined wave patterns for $p = 0$ overlap with instabilities of the flow when $p > 0$. Therefore, the dawdling probability p has a significant impact

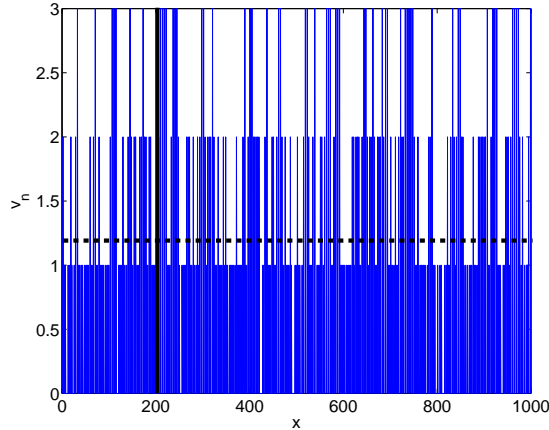


Figure 8: Trivial flow solution for bottleneck simulation with average density $\rho > 0.25$ (here: $\rho = 0.45 \Rightarrow d \approx 2.22$). The average speed $v \approx 1.22$ is visualized by the thick dotted line. The average flux is exactly at $q = 1 - \rho = 0.55$, as expected from a trivial flow solution in the fundamental diagram. Even on the open-road segment the speed does not exceed $v_B^{max} = 3$. Therefore, the bottleneck has no longer an impact on the flow solution.

on the effective fundamental diagram, which is defined as the average flux on the bottleneck loop versus the average density, as shown in Fig. 9. It shows three separate values of p ($p = 0.0; 0.2; 0.5$). To plot the figure, the parameters were chosen as $L = 1000$, $L_B = 200$, $v^{max} = 5$ and $v_B^{max} = 2$. As the dawdling probability is increased, there is a decline in the flux for both parts of the road. This is expected since the vehicles are more likely to reduce their speed randomly as p increases. The flow also becomes more unstable.

When $p = 0$, it can be shown analytically that the effective FD is piecewise linear and consists of three segments, joined at the critical values $\rho_{c1} = 13/75 \approx 0.1733$ and $\rho_{c2} = 1/3$. These three linear regimes correspond to the three wave patterns found in the previous section. The critical values for ρ are determined in a fashion similar to the critical density values in section 3. The linear function

$$Q(\rho) = \frac{50}{13}\rho \quad (11)$$

for $0 \leq \rho \leq 13/75$ is also derived from conservation of cars and zero wave

speed. The intermediate constant function, determined by the maximum of q_B for case 1 in Fig. 3, then joins onto the FD of the open road (no bottleneck; $L_B = 0$). Hence, we have a complete understanding of the effective FD for a bottleneck with $p = 0$.

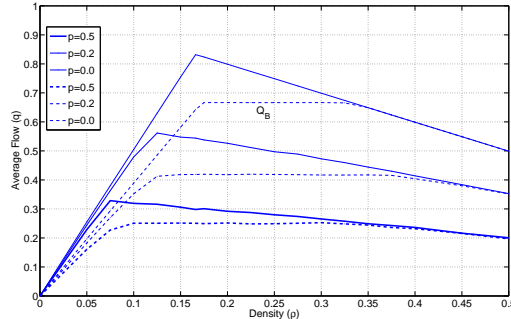


Figure 9: Effective fundamental diagrams (dashed lines) for three different values of the dawdling probability p from a simulation with $L = 1000$, $L_B = 200$, $v^{max} = 5$ and $v_B^{max} = 2$. Three distinct regimes can be identified. For comparison, the FD for the same simulations without a bottleneck (solid line; $L_B = 0$) exhibit only two distinct regimes.

However, for $p > 0$ we resort to numerical results only which again exhibit three distinct regimes, or phases, with rather blurry transitions between them. The occurrence of such three phases has been discovered in previous CA simulations and will we address some of these in section 6.

5 Link to optimal-velocity models

While the above first-order analysis explains the transition between the three wave patterns which are observed in the numerical simulations, it does not answer why they are selected or why the remaining wave patterns in Fig. 3 do not occur. In this section, we will draw a parallel to the microscopic car-following optimal-velocity (OV) model. We will simulate a bottleneck in the OV model in a way similar to the CA model and analyze how it compares to the CA results. It turns out that the same three wave patterns appear again and occur exclusively. Using the corresponding continuum model, we can explain this phenomenon with second-order analytical methods.

5.1 Bottleneck simulation in the OV model

In the optimal-velocity model [22], the acceleration of each vehicle is determined by an equation of motion that includes an optimal (or desired) velocity V which depends on the distance, $h_n = \Delta x_n$, to the preceding vehicle.

The governing equation reads

$$\ddot{x}_n = a[V(\Delta x_n) - \dot{x}_n] \quad (12)$$

where $\Delta x_n = x_{n+1} - x_n$, and n denotes the index of each vehicle at position x_n . The velocity is represented by \dot{x}_n and acceleration by \ddot{x}_n .

In order to be consistent with the CA model, we use a piecewise linear optimal-velocity function with a maximum velocity in the bottleneck at 60% of the maximum velocity on the open road, again shown qualitatively in Fig. 2. For simplicity, we used $v_B^{max} = 0.6$ and $v^{max} = 1.0$ with an offset $h' = 0.1$, representing the distance a vehicle occupies in a jam. Note that we are working with a dimensionless model just as it was the case for the CA model.

This results in an optimal-velocity function (bottleneck: subscript B ; open road: subscript o)

$$V_B(h) = \begin{cases} h - 0.1 & ; h < 0.7, \\ 0.6 & ; h \geq 0.7 \end{cases} \quad (13)$$

$$V_o(h) = \begin{cases} h - 0.1 & ; h < 1.1, \\ 1.0 & ; h \geq 1.1 \end{cases} \quad (14)$$

and the fluxes

$$q_B = \begin{cases} 1 - 0.1\rho & ; \rho > 1/0.7, \\ 0.6\rho & ; \rho \leq 1/0.7 \end{cases} \quad (15)$$

$$q_o = \begin{cases} 1 - 0.1\rho & ; \rho > 1/1.1, \\ \rho & ; \rho \leq 1/1.1. \end{cases} \quad (16)$$

The sensitivity a is chosen so that we guarantee linear stability. The flow stability is determined by [22]

$$V'(h) < a/2, \quad (17)$$

which also defines a range of headways for which the model is unstable. For the simulations performed, $a = 2.0$ was chosen to maintain stable flow.

Initially, we place N vehicles randomly along a loop of length L with a bottleneck of length L_B and let the system evolve.

5.2 Wave selection in the fundamental diagram

Using the above equations for the flux in the bottleneck and on the open road, the fundamental diagram is (qualitatively) identical to that of the CA model in Fig. 3. After a variety of simulations are carried out, the same three wave patterns which occurred in the CA model, also emerge in the OV model, while other wave patterns never appear. These three wave patterns also form three traffic phases which are qualitatively identical to those of the CA model (see Fig. 9).

We find: i) Two shocks at low density, one occurring at either end of the bottleneck, corresponding to case 2 in the CA model; ii) two shocks at medium density, one occurring at the upstream bottleneck boundary and one (classical Lax shock) appearing on the open road (case 1 in the CA model); iii) uniform, homogeneous flow (case 3 in the CA model).

These numerical results, including the critical densities of each regime, can again be discussed with first-order analytical methods, namely conservation of cars and zero wave speed, i.e. kinematic wave theory. This analysis explains again the connection between the wave patterns observed in the (OV) model but it does not explain why these are the only wave connections selected in Fig. 3. In order to investigate this phenomenon in more detail, we will now use continuum theory and analyse the travelling-wave phase plane of the continuum analogue of the OV model.

5.3 Travelling-wave phase-plane analysis

Previous work in continuum theory by Berg *et al.* [12] and Lee *et al.* [13] will now be used to analyse the travelling-wave patterns expected from the fundamental diagram of the OV model and, hence, the CA model. A priori, it is unclear whether wave patterns may occur in the OV model which cannot be found in the CA model. Hence, second-order continuum theory will be applied to analyse *all* plateau connections in the OV model.

Lee *et al.* [13] derived a second-order continuum model of the OV model, using density ρ and velocity v as the two variables. Using the conservation of cars

$$\rho_t + (v\rho)_x = 0 \tag{18}$$

and the dynamic equation involving the optimal velocity

$$v_t + vv_x = a[\hat{V}(\rho) - v] + \frac{a\hat{V}'(\rho)}{2\rho}\rho_x + \frac{a}{6\rho^2}v_{xx}, \tag{19}$$

the stability of the shock tails will now be analysed, meaning the stability of the equilibrium points (EP) in the corresponding travelling-wave phase plane. Here, we define $\hat{V}(\rho) = V(1/\rho) = V(h)$.

5.3.1 Phase-plane analysis under constant optimal velocity

A constant optimal velocity, $\hat{V}'(\rho) = 0$, refers to the positive slopes of the fundamental diagram where the flux is found from $q = v^{max}\rho$ in Eqs. (15)–(16). Therefore, we have $V(h) = V(1/\rho) = \hat{V}(\rho) = v^{max}$ and $\hat{V}'(\rho) = 0$, where v^{max} is the constant maximum optimal velocity. Note that the same analysis is applied to the bottleneck regime by substituting v_B^{max} for v^{max} .

With these parameters and assuming stationary shock waves ($v_t = \rho_t = 0$), Eq. (19) becomes

$$vv_x = a[v^{max} - v] + \frac{a}{6\rho^2}v_{xx}. \quad (20)$$

Using the definition for the flux, $q = v\rho$, and linearization via $v = v^{max} + \hat{v}$ yields

$$v^{max}\hat{v}_x = -a\hat{v} + \frac{av^{max2}}{6q^2}\hat{v}_{xx}. \quad (21)$$

Here, the flux q is given by the boundary conditions at infinity.

This equation can now be written as two first-order ordinary differential equations

$$v_x = w, \quad (22)$$

$$w_x = \frac{6q^2}{av^{max2}}[v^{max}w + av], \quad (23)$$

where we have dropped the “hat” notation for v .

To find the stability of the equilibrium points, the eigenvalues of the preceding equations are found by rewriting the equations in matrix form

$$\begin{pmatrix} v_x \\ w_x \end{pmatrix} = \begin{pmatrix} 0 & 1 \\ \frac{6q^2}{v^{max2}} & \frac{6q^2}{av^{max2}} \end{pmatrix} \begin{pmatrix} v \\ w \end{pmatrix}. \quad (24)$$

Trying the ansatz $v, w \sim \exp(\lambda x)$, this yields the following two roots of the characteristic equation

$$\lambda_{1,2} = \frac{3q^2}{av^{max}} \pm \sqrt{\left(\frac{3q^2}{av^{max}}\right)^2 + \frac{6q^2}{v^{max2}}}. \quad (25)$$

Since $q, v^{max} > 0$ holds, the root is always larger than the term preceding the root and the eigenvalues represent a saddle in the phase plane of v and v_x . This allows wave connections both i) from an upstream plateau (equilibrium point) to this equilibrium point, representing the second plateau, along the stable manifold and ii) from this plateau to another plateau along the unstable manifold. Hence, wave connections are possible along the positive slopes of the fundamental diagram, as in case 2 in Fig. 3, which can now be interpreted as a saddle-saddle connection.

5.3.2 Phase-plane analysis for an optimal velocity dependent upon headway

An analysis is now performed for the monotonically decreasing part of the fundamental diagram where the OV function does vary with headway and, consequently, with density. Here, we have $V(h) = \hat{V}(\rho) = 1/\rho - 0.1$. The same analysis is carried out as before, however, this time for the dynamical equation

$$vv_x = a \left[\frac{1}{\rho} - 0.1 - v \right] - \frac{a}{2\rho^3} \rho_x + \frac{a}{6\rho^2} v_{xx}. \quad (26)$$

Using $q = v\rho$ again, and hence $\rho_x = \frac{-qv_x}{v^2}$, we obtain

$$vv_x = a \left[\left(\frac{1}{q} - 1 \right) v - 0.1 \right] + \frac{av}{2q^2} v_x + \frac{av^2}{6q^2} v_{xx}. \quad (27)$$

Now let $v = \bar{v} + \hat{v}$ and $\bar{v} = \frac{0.1}{1/q-1}$, we find

$$\bar{v}\hat{v}_x = a \left(\frac{1}{q} - 1 \right) \hat{v} + \frac{a\bar{v}}{2q^2} \hat{v}_x + \frac{a\bar{v}^2}{6q^2} \hat{v}_{xx}. \quad (28)$$

Writing this again in terms of two first-order differential equations, we obtain

$$v_x = w, \quad (29)$$

$$w_x = \frac{6q^2}{a\bar{v}^2} \left[\bar{v} \left(1 - \frac{a}{2q^2} \right) w - a \left(\frac{1}{q} - 1 \right) \hat{v} \right]. \quad (30)$$

To find the stability of the equilibrium points, the eigenvalues of the preceding equations are determined via matrix notation

$$\begin{pmatrix} v_x \\ w_x \end{pmatrix} = \begin{pmatrix} 0 & 1 \\ \frac{6q^2}{\bar{v}^2} \left(1 - \frac{a}{2q^2} \right) & \frac{6q^2}{a\bar{v}} \left(1 - \frac{a}{2q^2} \right) \end{pmatrix} \begin{pmatrix} v \\ w \end{pmatrix} \quad (31)$$

and so

$$\begin{aligned} \lambda_{1,2} &= \frac{3q^2}{a\bar{v}} \left(1 - \frac{a}{2q^2}\right) \\ &\pm \sqrt{\left[\frac{3q^2}{a\bar{v}} \left(1 - \frac{a}{2q^2}\right)\right]^2 + \frac{6q^2}{\bar{v}^2} \left(1 - \frac{1}{q}\right)}. \end{aligned} \quad (32)$$

Since $0 < q < 1$ holds, it can be seen that $\left(1 - \frac{1}{q}\right) < 0$ and the argument under the square root can be positive or negative. In any case, stability is governed by the sign of the real part of $\lambda_{1,2}$ and that is always determined by $\frac{3q^2}{a\bar{v}} \left(1 - \frac{a}{2q^2}\right)$ since the root is either purely imaginary or real but smaller than $\frac{3q^2}{a\bar{v}} \left(1 - \frac{a}{2q^2}\right)$. Since $q, a, \bar{v} > 0$ holds, the real part will either be greater than or less than zero depending on the term $\left(1 - \frac{a}{2q^2}\right)$. If $a \geq 2$ and $0 < q < 1$, which is the case in our simulations (see Eqs. (15) and (16) where $q \leq 1/1.1$), the real part will be less than zero. Hence, the equilibrium point (EP) is a stable node (or spiral). Therefore, we can connect from an upstream plateau to this EP but we cannot connect from this EP to another equilibrium point downstream to form a wave pattern. This prevents the formation of patterns 3, 4 and 5 in Fig. 3, which would involve a non-permissible connection starting from an EP of the monotonically decreasing branch of the FD.

For the same reasons, case 1 in Fig. 3 must be considered as a limiting scenario of the above-mentioned saddle-saddle connection of case 2 between the monotonically increasing branch of the bottleneck FD and the open-road FD, respectively.

Future work will investigate a bottleneck simulation for unstable flow where $a < 2$ holds. Then it is possible to find unstable nodes in Eq. (32) since we can have

$$1 - \frac{a}{2q^2} > 1 \quad (33)$$

or, equivalently,

$$a < 2q^2. \quad (34)$$

5.3.3 Further thoughts

At this stage, it is unclear how the instability of the flow will affect the wave patterns and whether some stable wave patterns will persist.

Also, it should be noted that a similar bottleneck simulation with the (linearly stable) OV model [22] has been carried out by Wilson *et al.* [24, 25]. Here, the bottleneck was simulated by a reduction factor in the optimal-velocity function, resulting in new wave patterns. A coarse-graining method reveals that second-order theory might be insufficient to explain all wave patterns at the microscopic level. However, a higher-order continuum model is not available. Moreover, if one follows the idea of Berg *et al.* [12] and extended their continuum model to higher order, it would involve second-order (and higher) derivatives of $\hat{V}(\rho)$ and they all vanish for a piecewise linear OV function so that a higher-order modelling approach would fail in the context of this paper.

Furthermore, the continuum model of Berg *et al.* completely fails in explaining the saddle-saddle connections since one ends up with an insufficient first-order model

$$vv_x = a[v^{max} - v] \quad (35)$$

along those branches of the FD. This clearly shows the advantage of the Lee *et al.* model, adding to its advantage over the Berg *et al.* model in terms of matching the linear stability criterion of the discrete OV model at short wave lengths.

In summary, kinematic wave theory alone cannot fully explain the selection of stationary shocks in the bottleneck simulation. Surely, stationary wave patterns can be expected at the boundaries due to a non-smooth change in model parameters. However, it is the dynamics of the model which determine the actual observable patterns, and these resemble each other in the OV and CA model simulations. This includes the appearance of three traffic phases in either model.

6 Comparison to open-system and other non-homogeneous CA models

There have been several publications about CA models in the literature which contain either two [7], three [3, 6, 8, 5, 9] or several traffic phases [4], as defined in section 4.

Yukawa *et al.* [3] simulated a blockage on a loop in the rule-184 CA model, having a maximum speed $v^{max} = 1$. At exactly one site along the loop, the hopping probability of an otherwise deterministic model is reduced from $r = 1$ to $0 < r < 1$. The authors find three traffic phases, depending on the average traffic density and the hopping parameter r . In

order of increasing density, they are: i) free, ii) constant-flow and iii) jam phase. This resembles the three wave patterns in this work (see section 4), where the constant-flow phase is determined by $q_B^{max} = 3/4$ in the regime $0.17 \leq \rho \leq 0.25$. However, while the free phase in the rule-184 CA model is the same with or without a blockage site, this is not the case in our simulations. In addition, the present work considers a fully deterministic CA model and focuses on its emerging wave patterns. Moreover, the bottleneck simulations in section 3 will change as $L_B \rightarrow 1$ due to finite size effects since the formation of plateaus within the bottleneck will disappear. Therefore, planned future work will investigate how the limit $L_B \rightarrow 1$ will affect the results both for $v_B^{max} = 3$ and $v_B^{max} = v^{max} = 5$, and a non-zero dawdling probability $p > 0$ in the bottleneck only.

Lakatos *et al.* [9] extended the idea of Yukawa *et al.* to multiple blockage sites in a totally asymmetric simple exclusion process (TASEP) model on an open road. Approximate mean-field theory provides good agreement between the numerical results and Monte Carlo simulations. Phase diagrams are derived, which contain again three phases, but wave patterns are not discussed due to the lack thereof. More importantly, the boundary conditions mainly drive the dynamics of this open system, which brings us to the next set of simulations.

The stationary wave patterns of the present bottleneck simulation would change dramatically if the loop was replaced by an open road with fixed but different up- and downstream boundary conditions [4, 5, 6, 7, 8]. The constraint of conservation of cars, which enables the analytical computations of phase boundaries between the three wave patterns (see also [3]), disappears and the analysis of the model becomes more challenging. Depending on the model, three [5] or more phases [4] can be found. Here, stationary wave patterns are determined by the boundary conditions alone and can even be triggered in an otherwise stable model, with or without a bottleneck. In contrast, such patterns may or may not exist on the loop, depending on the stability of the model. This fundamental difference is exhibited for the OV model on a loop and open road by the work of Bando *et al.* [22] and Berg *et al.* [26], respectively. Therefore, future work will also investigate the bottleneck setup of the present paper under open-system boundary conditions similar to [4, 5, 6, 7, 8].

7 Conclusion and future work

In this paper, the dynamics of a bottleneck simulation exhibit a link between cellular automata and optimal-velocity traffic models. Three wave patterns, which correspond to three distinct traffic phases in the fundamental diagram, occur in either model and are qualitatively identical. This is surprising in some sense since it connects a model, which is discrete in space and time, to a model, which is continuous in space and time. The emerging wave patterns were analysed and explained with second-order continuum theory.

Future work will focus on a CA model with non-zero dawdling probabilities $0 < p < 1$. However, this entails the formation of jams, which overlap with the stationary wave patterns. On the other side, similarities to the work of Yukawa *et al.* [3] can be expected to emerge from these simulations.

Moreover, the stationary wave patterns which occur on a long straight road, containing a bottleneck and different up- and downstream boundary conditions, will be studied. Here, travelling waves cannot interact multiple times with stationary patterns. This should give rise to new wave solutions as compared to the loop, determined by the boundary conditions. This resembles research presented in [5, 6, 8] but is fundamentally different from what was presented in this work.

Acknowledgement

Peter Berg is supported by an NSERC Discovery Grant. We would like to thank Y. Sugiyama for bringing bottleneck simulations to the authors attention, B.S. Kerner and R.E. Wilson for the valuable discussions.

References

- [1] A. Schadschneider, *Physica A* **285**, 101 (2000)
- [2] B. Kerner, S. Klenov and D. Wolf, *J. Physics A: Mathematical and General* **35**, 9971 (2002)
- [3] S. Yukawa, M. Kikuchi and S. Tadaki, *J. Phys. Soc. Japan* **63**, 3609 (1994)
- [4] V. Popkov and G. Schuetz, *Europhys. Letters* **48**, 257 (1999)
- [5] A. Kolomeisky, G. Schuetz, E. Kolomeisky and J. Straley, *J. Phys. A: Math. Gen.* **31**, 6911 (1998)

- [6] S. Cheybani, J. Kertesz and M. Schreckenberg, Phys. Rev. E **63**, 016108 (2001)
- [7] S. Cheybani, J. Kertesz and M. Schreckenberg, Phys. Rev. E **63**, 016107 (2001)
- [8] R. Barlovic, T. Huisinga, A. Schadschneider and M. Schreckenberg, Phys. Rev. E **66**, 046113 (2002)
- [9] G. Lakatos, T. Chou and A. Kolomeisky, Phys. Rev. E **71**, 011103 (2005)
- [10] K. Nagel and M. Schreckenberg, J. Phys. I France **2**, 2221 (1992)
- [11] A. Schadschneider and M. Schreckenberg, J. Phys. A: Math. Gen. **26**, L679 (1993)
- [12] P. Berg, A. Mason and A. Woods, Phys. Rev. E **61**, 1056 (2000)
- [13] H.K. Lee, H.W. Lee and D. Kim, Phys. Rev. E **64**, 056126 (2001)
- [14] D. Helbing, *Verkehrsdynamik: Neue physikalische Modellierungskonzepte*, (Springer, Heidelberg, 1997)
- [15] B. Kerner, *The Physics of Traffic*, (Springer, Heidelberg, 2004)
- [16] B. Kerner, Phys. Rev. E **65**, 046138 (2002)
- [17] B. Jia, R. Jiang and Q. Wu, Phys. Rev. E **69**, 056105 (2004)
- [18] Y. Sugiyama, A. Nakayama, M. Fukui, K. Hasebe, M. Kikuchi, K. Nishinari, S. Tadaki and S. Yukawa, in *Traffic and Granular Flow '03*, edited by S.P. Hoogendoorn, S. Luding, P.H.L. Bovy, M. Schreckenberg and D.E. Wolf, (Springer, Heidelberg, 2005), p. 45
- [19] B. Kerner and S. Klenov, Phys. Rev. E **68**, 036130 (2003)
- [20] P. Berg and A. Woods, Phys. Rev. E **64**, 035602 (2001)
- [21] D. Helbing, A. Hennecke and M. Treiber, Phys. Rev. E **82**, 4360 (1999)
- [22] M. Bando, K. Hasebe, A. Nakayama and Y. Sugiyama, Phys. Rev. E **51**, 1035 (1995)
- [23] G.B. Whitham, *Linear and Nonlinear Waves*, (Wiley Inter-Science, New York, 1999), p. 68

- [24] J. Ward, E. Wilson and P. Berg, in *Traffic and Granular Flow '05*, edited by A. Schadschneider, T. Poeschel, R. Kuehne, M. Schreckenberg and D.E. Wolf (Springer, Heidelberg, 2007), p.565
- [25] J. Ward, E. Wilson and P. Berg, *Physica D*, accepted (2007)
- [26] P. Berg and A. Woods, *Phys. Rev. E* **63**, 0361907 (2001)